ACS SENSORS

Article

Cite This: ACS Sens. 2019, 4, 3166−3174

pubs.acs.org/acssensors

Avidity-Based Affinity Enhancement Using Nanoliposome-Amplified SPR Sensing Enables Low Picomolar Detection of Biologically Active Neuregulin 1

Namik Akkilic,[†] Mathias Liljeblad,[‡] Stefan Blaho,[§] Mikko Hölttä,[∥] Fredrik Höök,[⊥] and Stefan Geschwindner*[,†]

[†]Structure, Biophysics and Fragment-based Lead Generation, Discovery Sciences, [‡]Translational Science & Experimental Medicine, Early Cardiovascular, Renal and Metabolism, [§]Protein Science, Discovery Biology, Discovery Sciences, [∥]Clinical Pharmacology Biologics and Bioanalysis, Clinical Pharmacology & Safety Sciences, BioPharmaceuticals R&D, AstraZeneca, Gothenburg 431 50, Sweden

[⊥]Department of Applied Physics, Division of Biological Physics, Chalmers University of Technology, Gothenburg 412 96, Sweden

Supporting Information

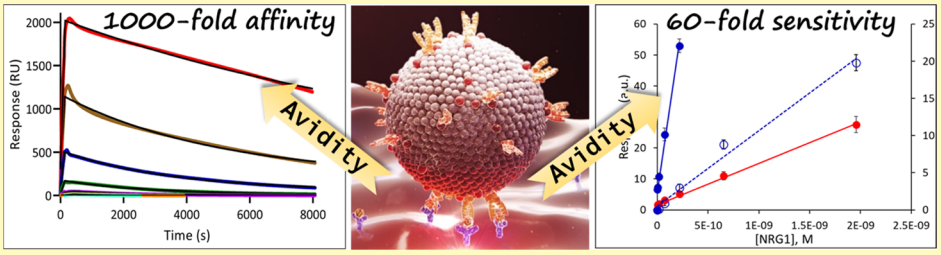

ABSTRACT: Biomarkers serve as indicators of disease progression or therapeutic response of an medical intervention, and means for enabling a reliable and sensitive biomarker detection are therefore vital in clinical settings. Most biosensor assays require high-affinity interactions in combination with an enzyme or fluorescent tag to enable detection and frequently employ extensive washing procedures prior to signal readout. Attempts to overcome this limitation by using natural biological partners tend to be demanding, because their very low affinity is frequently not compatible with the need of reaching low limits of detection (LODs), especially for circulating biomarkers that possess short half-lives. To address these challenges, we developed a label-free surface plasmon resonance (SPR) platform for the detection of neuregulin 1 (NRG1) using ErbB4-modified liposomes offering both signal amplification and affinity enhancement via functional multivalent interactions. Through the functional avidity interaction between NRG1 and ErbB4, an LOD of 3.5 picomolar was reached, which is about 60-fold higher than traditional SPR and miniaturized immunoassays. The biosensor displays also an 8-fold higher sensitivity when compared with a single-molecule immunoassay employing the natural binding partner rather than a high-affinity antibody as one of the interaction partners. In fact, the liposome-induced avidity between NRG1 and ErbB4 offered an LOD that was comparable to that obtained using a high-affinity antibody and enabled detection of NRG1 in plasma with a LOD of 36 pM. Employing the liposome-enhanced platform in conjunction with a low-affinity biomarker receptor thus enables the assessment of the functional state of the biomarker at competitive LODs and eliminates the need for high-affinity antibodies.

KEYWORDS: *surface plasmon resonance, liposome, avidity, receptor, neuregulin, biosensing, biomarker*

Sensitive detection of biomarkers is vital as they are the indicator of cause, progression, and regression of a disease and thus can be used for early diagnosis or to follow pharmacological responses to therapeutic interventions and treatment follow-up.[1,2] However, biomarkers are often present at very low concentrations in complex biological matrices where they have highly variable concentrations, especially during disease states. They are often also subject to rapid turnover, resulting in multiple more or less functional variants. One such example is neuregulin 1 (NRG1), which is a key biomarker for several disease indications and carries a small fragment EGF-like domain exhibiting short half-life in circulation that limits its potential to be used for therapeutic purposes. To circumvent this problem when employing NRG1 as a biological treatment modality for metabolic homeostasis, NRG1 can be tagged with a Fc domain of human IgG1 which has been shown to exhibit prolonged plasma half-life of up to 40 h.[3] It has been shown that Fc-NRG1 can trigger potent AKT activation in the liver, enhance insulin sensitivity and glucose tolerance, and suppress food intake in obese mice.[3]

The NRG1 action is triggered by binding through its EGF-like domain and activates ErbB3 (HER3) and ErbB4 (HER4)

Received: July 24, 2019
Accepted: November 14, 2019
Published: November 14, 2019

DOI: 10.1021/acssensors.9b01392
ACS Sens. 2019, 4, 3166−3174

receptor tyrosine kinases. NRG1 specifically acts on ErbB4 which is the only autonomous NRG1-specific ErbB. Through the interaction with the ErbB4 receptor, NRG1 can induce the growth and differentiation of epithelial, neuronal, glial, and other types of cells.[4] NRG1−ErbB4 signaling has been linked to developmental abnormalities and pathogenesis of multiple diseases as it is essential during the development of the nervous system[5] as well as cardiac development and functional integrity of the heart.[6,7] Particularly, NRG1−ErbB4 signaling plays a fundamental role in complex brain disorders such as pathophysiology of schizophrenia,[8,9] pathogenesis of amyotrophic lateral sclerosis,[10] pathological development of Alzheimer's disease (AD),[11] bipolar disorder, and depression.[5] Mice-model experiments showed a direct correlation of total axonal NRG1 levels with the myelin sheath thickness.[12] Furthermore, increased levels of NRG1 expression and reduced phosphorylated ErbB4 receptor levels were found in the frontal lobe of a patient with AD.[11] On the other hand, ErbB4 can be overexpressed in head and neck cancer while downregulated in papillary carcinoma and high-grade gliomas, as well as lung, renal, and breast cancer.[13,14] Thus, NRG1 and its interactions with the ErbB4 receptor can serve as an ideal diagnostic reporter for drug development especially for neuronal diseases, heart failure, and several cancer types.

In common for assays designed for the purpose of monitoring the concentration of NRG1 and other low abundant and fragile biomarkers is the requirement for low detection limits, where so called digital single-molecule platforms have demonstrated impressive promise.[15,16] The Erenna immunoassay system (Singulex Inc.) overcomes the sensitivity and specificity issues of conventional ELISA by utilizing microbead-based immunoassays that count fluorescently labeled detection antibodies which are directly proportional to the amount of the target analyte present in the sample. This format was applied to quantify cardiac troponin I and various cytokines with a limit of detection (LOD) from 10 to 100 pg/mL in 100 μL of sample.[17−19] Another ultrasensitive enzyme-linked digital immunoassay technology with a fully automated single-molecule array (Simoa from Quanterix Corporation) was introduced in 2010 that applies enzyme and fluorescent substrates as a functional read-out.[20] The Simoa technology digitally counts the number of wells containing both a bead and fluorescent product. Its sensitivity increase over conventional ELISA can be up to >1200-fold.[21] This bead-based ELISA technology has been applied to detect various biomolecules with the capability of multiplexing in human plasma in the range of 0.01−0.03 pg/mL.[22−27] Because of extensive rinsing steps prior to the signal readout, these assays have in common that they require two high affinity antibodies and an enzyme/fluorescent tag amplification chemistry for detection.[15,16]

Even though the high-affinity antibodies typically used in these assays are excellent in the context of reaching low detection limits, they may fail to discriminate functional from dysfunctional states of rapidly circulating biomarkers. This could be easily overcome by replacing at least one of the antibodies in conventional immunoassays by a natural interaction partner; however, the affinities of such interactions tend to be orders of magnitude lower than that of high-affinity antibodies, which in turn has devastating influence on the LOD. In this work, we demonstrate how this challenge can be overcome by increasing the affinity of natural interaction partners using multivalent interactions, accomplished by replacing one of the antibodies in conventional assays designed for NRG1 detection with liposomes decorated with its natural interaction partner ErbB4. To verify the feasibility of the concept, we employed surface plasmon resonance (SPR) spectroscopy, which allows us to directly access information on how the interaction kinetics is influenced by the degree of multivalency. The interaction strength was optimized by tuning the coverage of his-tagged ErbB4 to Ni^{2+}-NTA modified liposomes with a diameter of 90 nm. In particular, sufficiently fast association and slow dissociation kinetics between NRG1 and ErbB4-coated liposomes was defined as a hallmark of increased affinity mediated through avidity effects. The resulting LOD using liposomes as avidity and signal amplification elements using conventional SPR as the readout principle was 3.5 pM, which is ∼60-fold more sensitive than conventional tools such as miniaturized immunoassay, while the corresponding improvement was 8-fold compared to single-molecule digital platform, when for the latter ErbB4 was used as one of the recognition elements. Furthermore, because the sensitivity of low-affinity natural interactions is in this way boosted through liposome-induced functional avidity, our sensor can access differences in the functional states of rapidly circulating biomarkers with an LOD comparable to that of conventional immunoassays that employs two high-affinity antibodies which tend to reduce the capacity to distinguish different functional states of biomarkers.

EXPERIMENTAL SECTION

Materials. Unless otherwise stated, all chemicals were purchased from Sigma-Aldrich. All lipids were purchased from Avanti polar lipids. Human ErbB4 receptor was purchased from Acro Biosystems (Cat. no: ER4-H5221) and dissolved as per the manufacturer's protocol. CaptureSelect Biotin Anti-IgG-Fc was purchased from Thermo Fisher Scientific.

Expression of Fc-NRG1 and NRG1-ab. Fc-NRG1 was purified in an endotoxin-free environment at 4 °C. In brief, the protein was overexpressed and secreted into the media using HEK293 cells. The media was cleared by centrifugation at 4000 rpm for 15 min. MabSelect resin was directly added to the cleared cell culture media and left overnight at 4 °C with gentle agitation. The MabSelect resin was packed on a column, washed with buffer until the chromatogram baseline was stable and bound protein was released by an elution step with a glycine buffer at pH 3. The protein was concentrated for 2 h at 3400*g* (Beckman Coulter—Allegra 25R centrifuge) using Amicon spin tubes with a 30 kDa cut off. Finally, the concentrated protein was applied on a SEC 26/60 S200 (GE Healthcare) gel filtration column and collected. Anti-NRG Monoclonal Hybridoma Antibody (AZN-4-5) was purified using a 5 mL protein A affinity purification in PBS. The final concentration was 2.025 mg/mL.

Generation of NTA Liposomes. Liposomes composed of 96.5 wt % 1-palmitoyl-2-oleoyl-*sn*-glycero-3-phosphocholine, 2.5 wt % 1,2-dioleoyl-*sn*-glycero-3-[(*N*-(5-amino-1-carboxypentyl)iminodiacetic acid)succinyl] (DGS-NTA), and 1 wt % 1,2-dipalmitoyl-*sn*-glycero-3-phosphoethanolamine-*N*-(lissamine rhodamine B sulfonyl) (PE-Rho) with a total lipid mass of 2 mg were dissolved in 1 mL of chloroform in a small round beaker and subsequently dried in a nitrogen environment for at least 1 h. Lipid mixtures were rehydrated in HBS-N buffer [0.01 M 4-(2-hydroxyethyl)-1-piperazineethanesulfonic acid (HEPES) pH 7.4, 0.15 M NaCl] (GE Healthcare) containing 1 mM Ni^{2+} at 1 mg/mL and extruded at least 21 times through a 30 nm polycarbonate membrane (Whatman). To remove the free nickel ions, a Nap-10 column was used. We show the size distribution of liposomes in Figure S1, which is $Z_{average}$ = 90 nm and PdI = 0.2. The average size of the liposomes was determined using Zetasizer APS2000 (Malvern) from three independent measurements.

Liposome-Amplified SPR Assay. The assay has been conducted on a Biacore 2000 instrument (GE Healthcare) at 20 °C. The capture

DOI: 10.1021/acssensors.9b01392
ACS Sens. 2019, 4, 3166−3174

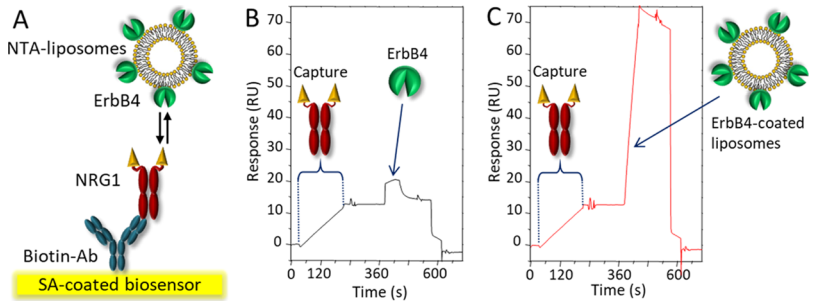

Figure 1. (A) Schematic depiction of the liposome-enhanced detection of NRG1 using the SPR biosensor. A SA-coated, 30 nm thick sensor chip is employed to tether a biotinylated antibody that is directed against the CH3 domain of human IgG-Fc. The Fc-tagged NRG1 can be subsequently captured through this antibody with a steady-state affinity of 5 nM (see Figure S3), thus resulting in a stable binding signal. Ni^{2+}-NTA liposomes that have been coated with ErbB4 have been employed in the next step to assess the functional concentrations of the captured Fc-NRG1. As SPR is a mass-sensitive method, enhancer elements that increase the mass of the analyte can boost the sensitivity tremendously. The SPR sensorgram for (B) injection of 200 pM Fc-NRG1 for 180 s followed by 60 s injection of 2.5 μM ErbB4. (C) ErbB4-coated liposomes binding to NRG1 (red curve). Injection of 200 pM Fc-NRG1 for 180 s followed by 60 s injection of 150 nM ErbB4 coated to 125 μg/mL Ni^{2+}-NTA liposomes before regenerating the biosensor surface.

antibody (CaptureSelect Biotin Anti-IgG-Fc) that is provided in a biotinylated form was tethered onto a streptavidin (SA)-coated (SAHC 30m, XanTec) sensor chip to a level of ~3000 RU using HBS-P buffer (0.01 M HEPES pH 7.4, 0.15 M NaCl, 0.005% v/v P20). In order to ensure controlled directionality of the Fc-NRG1 tethering, among a set of Fc-directed antibodies that are tested, the biotinylated anti-IgG-Fc (Hu) conjugate worked best in terms of binding stability and sensitivity (data not shown). After capture of the biotinylated antibody, the surface was blocked with 10 μg/mL biotin for 120 s via two consecutive injections at a flow-rate of 20 μL/min.

For the affinity measurements in Figure 2, NRG1 was captured at 35−65 RU and then increasing levels of ErbB4 (0−600 nM) and NRG1ab (0−12 nM) and increasing levels of ErbB4 (0−150 nM)-coated to 200 μg/mL Ni^{2+}-NTA liposomes passed on the sensor chip at a flow-rate of 5 μL/min. The surface was regenerated with a 60 s injection of 100 mM glycine pH 2.1 followed by 10 μM CHAPS injection at a flow-rate of 30 μL/min in preparation for the next cycle. SPR data was analyzed using either a kinetic fit to the data applying a 1:1 binding reaction model or using the steady state data (only for NRG1 and ErbB4 interactions) for fitting a 1:1 binding model to the data. A global nonlinear fit applied to calculate NRG1 and ErbB4-coated liposome interactions using association then dissociation curve fitting in GraphPad Prism 8.0.

For the liposome-amplified detection, Fc-NRG1 was captured for 600 s at a flow-rate of 5 μL/min in 2× HBS-P buffer. Plasma samples have been diluted 25% with 2× HBS-P buffer and injected for 600 s at a flow-rate of 5 μL/min in 2× HBS-P to capture total NRG1. Plasma EDTA K2 has been obtained from male RCCHan:WIST rat (Envigo). The series of ErbB4-coated liposomes has been prepared by mixing 200 μg/mL Ni^{2+}-NTA liposomes with 50 nM ErbB4 receptor (his-tagged, ACRO Biosystems) (see Table S1) in HBS-N buffer and was subsequently injected over the surface for 2−5 min at a flow-rate of 5 μL/min to optimize the receptor binding competency of the captured material (Figure S2).

Gyrolab Miniaturized Immunoassay. NRG1 concentrations were measured using the Gyrolab miniaturized high-sensitivity immunoassay method (Gyros, Inc., Warren, NJ). NRG1 samples were diluted in Rexxip A Max buffer (Gyros AB, Inc. catalogue number P0004995) in a 96-well plate (Thermo Scientific catalogue number AB-800). The concentrations of the fluorescently labeled ErbB4 and NRG1ab were diluted to 0.26 and 0.08 nM in Rexxip F buffer (Gyros AB, Inc. catalogue number P0004825), respectively. The capture reagent biotinylated anti-Fc-IgG was prepared in PBS containing 0.01% Tween-20. Samples were sealed with microplate covers (Gyros AB, Inc., catalogue number P0003313) and mixed thoroughly in a plate shaker for 60 s. To remove the possible bubbles, plates were centrifuged at 1000 rcf for 300 s at 20 °C. After ensuring that there were no bubbles in the bottom of the wells, the samples were measured in a Bioaffy 1000 CD (Gyros AB, Inc., catalogue number P0004253) in the Gyrolab xP workstation. A 3-step C-A-D method was executed on the Gyrolab xP workstation: (1) capture antibody biotinylated anti-Fc-IgG was flowed through a column containing SA-coated particles, (2) followed by the analyte (NRG1) applied to activated columns in a parallel manner, one sample per column and (3) the detection antibody which is Alexa 647 labeled ErbB4 (AL647-ErbB4) or NRG1ab (AL647-NRG1ab) was applied to each column. The Gyrolab xP workstation performed washes of PBS containing 0.01% Tween-20 (Calbiochem, Inc. catalogue number 655206) in between each step. Visualization and measurements were achieved by laser-induced fluorescence detection at 647 nm. Alexa 647 fluorescence labeling was performed using a labeling kit (Invitrogen by Thermo Fisher, catalogue number A-20186) as per the manufacturer's protocol.

Erenna Paramagnetic Microparticle-Based Immunoassay. Singulex experiments were carried out using the Single Molecule Counting (SMC) Erenna Instrument (Singulex, Inc.). A method for the detection of Fc-NRG1 was developed by optimizing capture and detection reagent concentrations. The method was setup according to the protocol recommended by the manufacturer using SMC Bead-Based Immunoassay Development Buffer Kit (Merck, catalogue number 03-0078-00). Briefly, the capture antibody (biotinylated anti-Fc-IgG) was precoated onto paramagnetic microparticles (MPs) at a concentration of 12.5 μg/mg beads using standard procedures provided by the manufacturer (Merck, catalogue number 03-0077-02). The coated MP in assay buffer (5 mg/well) and 100 μL Fc-NRG1 in standard buffer or plasma were added into microplates, incubated for 2 h, and then washed. 20 μL of fluorescently labeled detection antibody (0.08 nM) or ErbB4 (0.26 nM) was added to each well and incubated for 2 h, followed by another wash step. Incubation with elution buffer released the labeled antibodies or receptors from the MPs, and the neutralized supernatant were transferred to the reading plate. The number of fluorescently labeled NRG1 antibodies or ErbB4 was detected and counted by the Erenna System (Singulex, Inc.), which is directly proportional to the amount of target analyte present in the sample upon capture.

RESULTS AND DISCUSSION

Creating a Capture SPR Assay with Liposomes. We created an SPR capture assay that enabled the determination of the concentration of NRG1 through binding to liposome-bound ErbB4. To enable full accessibility of the tethered ligand to the liposomes, the biotinylated capture antibody was attached onto a SA-coated sensor chip with low thickness (30 nm). The thin coating compared with the extension of the evanescent sensing depth (~150 nm) offered improved

DOI: 10.1021/acssensors.9b01392
ACS Sens. 2019, 4, 3166−3174

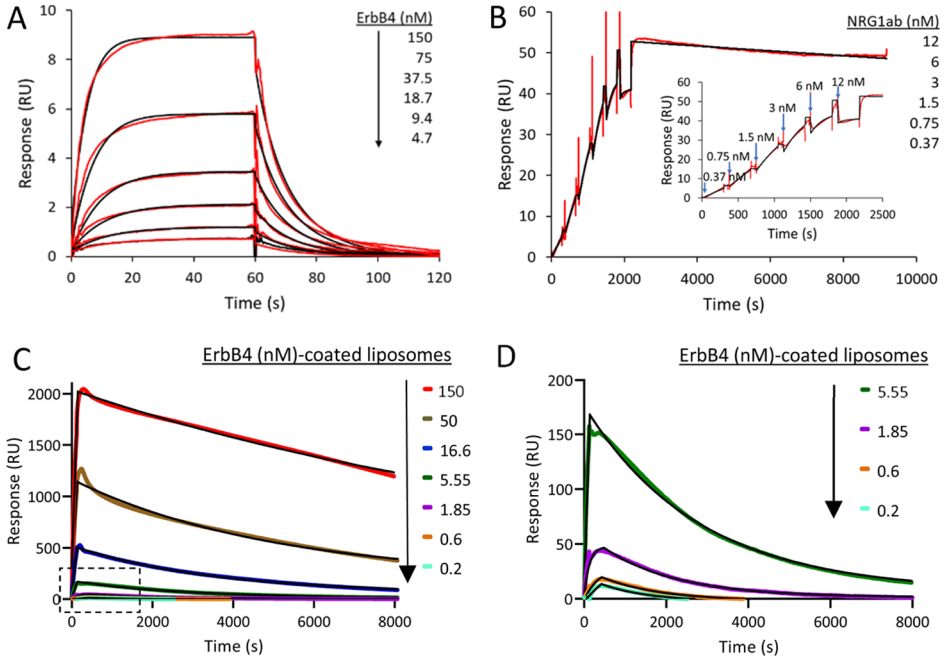

Figure 2. (A) Multicycle kinetics between NRG1 and ErbB4 (red curves). NRG1 binding level is 50 RU (bulk concentration 13 nM) to anti-Fc-antibody which is captured on a SA-coated biosensor. Increasing concentration levels of ErbB4 molecules (150 nM maximum ErbB4 with 1:2 dilution) have been passed over the sensor chip. Data was fitted (black curves) by applying a 1:1 binding reaction model (K_d = 127 nM) using the Biacore S200 Evaluation Software 1.0. (B) Single-cycle kinetic data (red curve) and fittings (black curve) for binding of NRG1ab to NRG1. NRG1ab (12 nM maximum with 1:2 dilution) was passed over the NRG1-bound (65 RU), SA-coated sensor chip. The inset shows the details of the association curves in the figure. The data is fitted to 1:1 binding model (black curve) using the Biacore S200 Evaluation Software 1.0. (C) Multicycle kinetics between NRG1 and ErbB4-coated liposomes. The NRG1 capture level is 35 RU at each cycle. Increasing concentration levels of ErbB4 molecules (150 nM maximum ErbB4 with 1:3 dilution) coated to 200 μg/mL liposomes were passed over the NRG1-attached sensor chip. (D) Zoomed in area (dashed square) in (C). Kinetic parameters were calculated from a non-linear fit of the data using GraphPad Prism. The data in the ErbB4 concentration regime between 5.5 and 150 nM were used to estimate the observed affinity K_d(obs).

Table 1. Affinity and Dissociation Rates for NRG1−ErbB4

construct	K_d (nM)	k_a (1/M s)	k_d (1/s)
NRG1−ErbB4	127 ± 6	$1 \times 10^6 \pm 1.9 \times 10^5$	$1.4 \times 10^{-1} \pm 1.7 \times 10^{-2}$
NRG1−NRG1ab	0.02 ± 0.007	$2.2 \times 10^6 \pm 1.9 \times 10^5$	$4.4 \times 10^{-5} \pm 1.2 \times 10^{-5}$
NRG1−ErbB4 coated liposome ([ErbB4] = 5.5−150 nM)	[a]0.07 ± 0.03	[a]$5.5 \times 10^6 \pm 2.4 \times 10^6$	$2.5 \times 10^{-4} \pm 2.0 \times 10^{-4}$
NRG1−ErbB4 coated liposome ([ErbB4] = 0.2−1.85 nM)	nd	nd	$1.0 \times 10^{-3} \pm 5.5 \times 10^{-5}$

[a]K_d(obs) = observed affinity, k_a(obs) = observed association rate, and nd = not determined, n = 3.

sensitivity for the liposome-enhancement step while simultaneously offering low unspecific binding of a liposome-bound analyte to the surface.

As SPR is a mass-sensitive method, enhancer elements that increase the mass of the analyte can boost the sensitivity tremendously.[28] By adapting from previous work,[28,29] Ni^{2+}-NTA liposomes that have been coated with ErbB4 have been employed to assess functional concentrations of NRG1 (Figure 1A). The assay allows the observation of the binding of NRG1 as well as binding of ErbB4 to be monitored in the same experimental cycle. For the proof-of-concept, we tested binding of ErbB4 and ErbB4-coated liposomes to surface-tethered NRG1 (Figure 1A). Injection of 200 pM Fc-NRG1 for 180 s resulted in about 13 RU binding to anti-Fc-antibody. Upon exposure of surface-bound NRG1 to 2.5 μM ErbB4 (Figure 1B), the response saturated at ∼7 RU, while upon addition of 125 μg/mL Ni^{2+}-NTA liposomes preincubated with 150 nM ERbB4 (Figure 1C), the response increased to ∼57 RU without reaching a saturation level. This shows that the SPR response is magnified more than 20 times when ErbB4 is attached to liposomes, which further increases to more than 100 times when employing much lower ErbB4 concentrations.

Avidity Effect on NRG1−ErbB4 Affinity with Liposomes. To measure the affinity between NRG1 and ErbB4, increasing concentrations of ErbB4 (150 nM maximum ErbB4 with 1:2 dilution) were passed over a NRG1-functionalized sensor chip to generate multicycle kinetic data as shown in Figure 2A. The Fc-NRG1 capture level on the Fc-tagged antibody was 50 RU. One-to-one binding reaction model fitting to the data resulted in 127 ± 6 nM moderate affinity between NRG1 and ErbB4 (Table 1). This result is consistent with earlier affinity measurements of ErbB4 with NRG1 at pH 8.0 (146 nM)[30] and pH 7.4 (179 nM).[31]

We then determined the interaction kinetics between NRG1 and NRG1 antibody (NRG1ab) to compare the affinity between NRG1 and ErbB4. Increasing concentrations of NRG1ab (12 nM maximum NRG1ab with 1:2 dilution) were passed over the Fc-NRG1-coated (65 RU) sensor to generate single-cycle kinetic data as shown in Figure 2B. SPR results confirmed the high affinity interactions between NRG1 and

DOI: 10.1021/acssensors.9b01392
ACS Sens. 2019, 4, 3166−3174

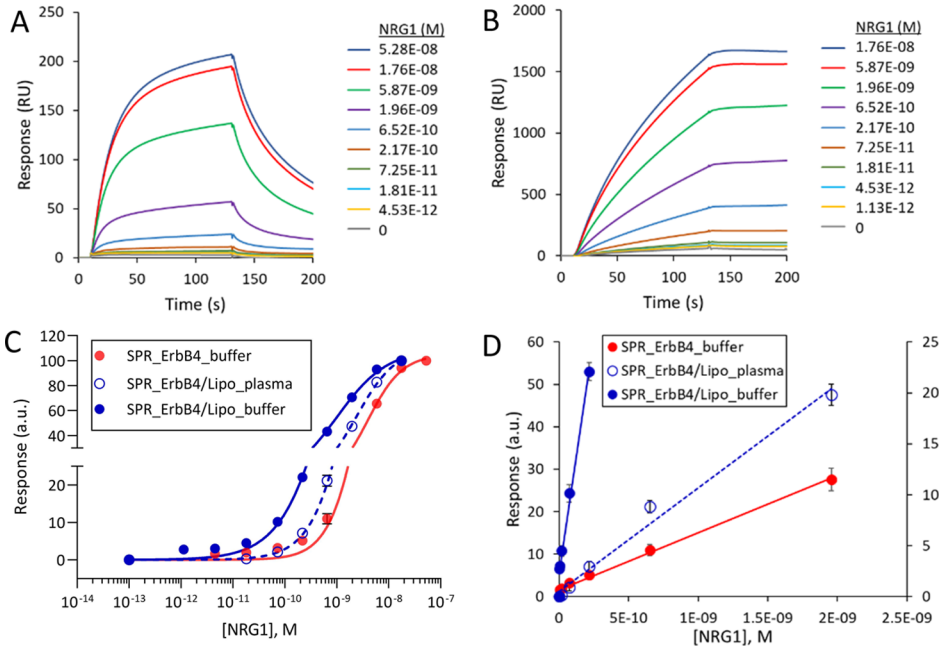

Figure 3. Liposome-enhanced SPR biosensor for NRG1 detection. Sensorgrams for (A) the interaction of 50 nM ErbB4 with increasing concentrations of NRG1 (0−17.6 nM, 1:3 dilution) (B) Interaction of 50 nM ErbB4 attached to 200 μg/mL liposome conjugates with increasing concentrations of NRG1 (0−17.6 nM, 1:3 dilution) at each cycle. (C) Dose−response curves and (D) linear relationship of the initial binding response of the NRG1 concentration from corresponding dose−response curves obtained after 120 s of injection of the analyte 50 nM ErbB4 in buffer (red circles), conjugation of 50 nM ErbB4 and 200 μg/mL liposome in buffer (blue, full circle) and in plasma (blue, open circle). Data normalized 0−100% in GraphPad Prism 8.0 and fitted to linear regression equation with $R^2 > 0.975$. The illustrated error bars represent the standard deviation of three repetitive measurements.

NRG1ab with a K_d = 0.02 ± 0007 nM from one-to-one binding reaction model fitting to the data (Table 1).

Figure 2C displays sensorgrams for increasing concentrations of receptor molecules (150 nM maximum ErbB4 with 1:3 dilution) being attached to a constant concentration of liposomes (lipid concentration 200 μg/mL) at each cycle. The NRG1 capture level (35 RU) was similar to the capture levels in Figure 2A,B. We calculated the association and dissociation rates between NRG1 and ErbB4 that are attached to liposomes using a nonlinear global fitting to the data using GraphPad Prism (Table 1). Albeit the observed association rate indicates mass transfer limitation, as seen in the diffusion-limited association curves, the signal enhancement reached to 250-fold as a consequence of multivalent interactions induced by the ErbB4 molecules that are coated on the liposomes (see in Figure S4). Simultaneous binding of two ErbB4 molecules to one NRG1 will most likely induce "forced proximity", that is, binding of one ErbB4 is expected to force the second tethered one on the liposome to stay close to its corresponding site.[32] This forced proximity favors binding of ErbB4, as well as rebinding as soon as it dissociates from that site, leading to an increase in the ErbB4 residence time. Also, this form of rebinding events increases the local surface concentration of the dissociated ErbB4 molecules on the liposomes, thereby increasing the probability for rebinding to its original target site.[32] Observed association rates (k_a(obs)) for our liposome-amplified ErbB4 assay showed similar values when compared to NRG1ab binding to NRG1, and at least 1 order of magnitude higher on-rates compared to natural receptor ErbB4 binding to NRG1 (Table 1). This avidity effect is much more obvious when we compared the dissociation rates (k_d) (Table 1). The dissociation rate for NRG1 and ErbB4 (Figure 3A) is 0.14 s^{-1}. However, the dissociation rate for NRG1 and ErbB4-coated liposomes at high receptor concentrations (>5.5 nM ErbB4) is 2.5 × 10^{-4} s^{-1}, indicating more than 3 orders of magnitude slower dissociation from the sensor when liposomes are employed as a signal enhancer and scaffold for ErbB4. At low receptor concentrations (<5 nM ErbB4), we observe a moderate 10-fold reduction in the rate of dissociation, which could be a consequence of a reduced avidity effect (see Figure S5). Nevertheless, even at those low concentrations of ErbB4, the observed rate of dissociation is still about a factor of 100 higher when compared to the rate of dissociation of the free ErbB4 as shown in Figure 2A, highlighting the presence of polyvalency even at very low levels of ErbB4.

SPR-Based NRG1 Biosensor. Sensor conditions were further optimized by preparing a series of ErbB4-coated liposomes by mixing Ni^{2+}-NTA liposomes with his-tagged ErbB4 receptor by keeping the receptor (or liposome) concentration constant and varying the liposome (or receptor) concentration (Figure S2). The maximum sensor response was obtained by mixing 50 nM ErbB4 with Ni^{2+}-NTA liposome at a lipid concentration of 200 μg/mL, which was therefore used to explore specific detection of Fc-NRG1.

Figure 3A displays sensorgrams for binding of ErbB4 (50 nM) to a sensor chip pre-exposed to increasing concentrations of NRG1 (0−52.8 nM max, 1:3 dilution). Figure 3B displays the same type of data but using ErbB4-coated liposomes (50 nM ErbB4 mixed with 200 μg/mL liposomes) at increasing concentrations of NRG1 (0−17.6 nM, 1:3 dilution). When liposomes are employed in the system, binding of ErbB4 to NRG1 is limited by mass transfer as clearly seen in the diffusion limited association curves (also in Figure 2C). The maximum response of NRG1 binding to ErbB4-coated liposome is ∼1600 RU (Figure 3B) and ∼1400 RU (Figure S6) in buffer and plasma, respectively. The maximum absolute

DOI: 10.1021/acssensors.9b01392
ACS Sens. 2019, 4, 3166−3174

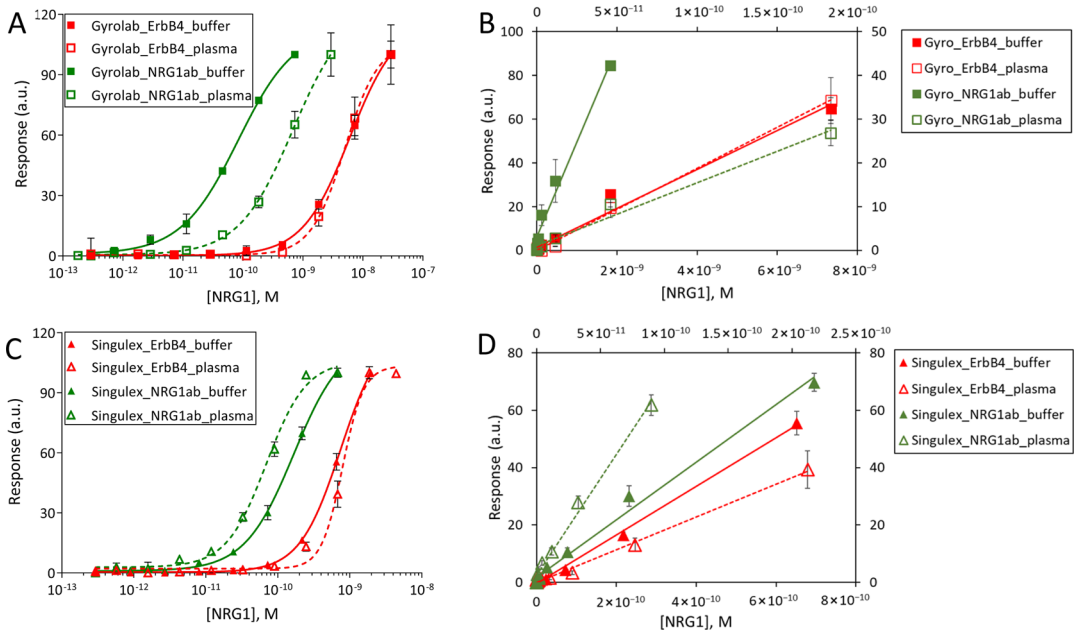

Figure 4. Gyrolab-detected (A) dose−response curves and (B) LOD for NRG1 binding to ErbB4 (red) and NRG1 binding to NRG1ab (green) in buffer (full square) and plasma (open square). Erenna (Singulex)-detected (C) dose−response curves and (D) LOD for NRG1−ErbB4 (red) and NRG1−NRG1ab (green) in buffer (full triangle) and plasma (open triangle). 0.26 nM ErbB4 or 0.08 nM NRG1ab labeled with AL647 fluorophore has been passed through the columns at each cycle for both Gyrolab and Singulex measurements. Data fitted to linear regression equation with $R^2 >$ 0.98. The illustrated error bars represent the standard deviation of three repetitive measurements.

response is significantly higher for ErbB4-coated liposomes (Figures 3B and S6) than for free ErbB4 (Figure 3A).

Because mass transfer limitations is a signature for slow diffusing molecules exhibiting fast binding reactions, the phenomenon could be used to determine concentrations from the linear regression curves at the boosted sensitivity, as they depict linearity in the initial binding responses. Figure 3C displays dose−response curves for ErbB4 binding to NRG1 in buffer (red) and ErbB4-coated liposomes binding to NRG1 in buffer (blue, full circle) and plasma (blue, open circle) conditions on logarithmic axis fitted to the Hill equation.[33] Under these conditions, binding of ErbB4-coated liposomes (50 nM ErbB4 and lipid concentration of 200 μg/mL) is linear up to 0.36 nM NRG1 concentration after which it exhibited an exponential behavior. In Figure 3D, the LOD for the detection of NRG1 was determined from the linear regression equation, through the 3σ rule (σ = standard deviation of the background signal). Employing free ErbB4, the LOD was 200 pM, whereas the LOD was improved to 3.5 pM in the presence of liposomes (n = 6). This represents about 60-fold enhanced sensitivity, which is attributed to the liposome-induced avidity effect for the interaction between ErbB4 and NRG1. The corresponding LOD upon liposome enhancement was for the plasma samples estimated to 36 pM. This is one order of magnitude higher than that of the obtained LOD using buffer conditions, which can be attributed to the increased background due to nonspecific binding of ErbB4-coated liposomes.

Gyrolab- and Singulex-Detected NRG1 Biosensor. To compare the liposome-enhanced assays with conventional diagnostic platforms, NRG1 was quantified using the Gyrolab miniaturized immunoassay method (Gyros, Inc., Warren, NJ) in dose−response curves shown in Figure 4A. First, the capture antibody (biotinylated anti-Fc-IgG) was flowed through a column containing SA-coated particles, followed by addition of NRG1 to activated columns in a parallel manner, one sample per column. The detection molecules, Alexa 647 labeled 0.26 nM ErbB4 (ErbB4-AL647) or 0.08 nM NRG1ab (NRG1ab-AL647), were subsequently applied to each column. The curves exhibit an S-shape which were fitted using the Hill equation describing the equilibrium behavior of reversible biomolecular binding. Using Gyrolab, we detected NRG1 when interacted with its natural receptor ErbB4 and NRG1ab both in buffer and plasma. To calculate the sensitivity of the assay, we show the calibration curves fitted with a linear regression equation in Figure 4B. The LOD is 198 and 0.6 pM for NRG1 binding to ErbB4 and NRG1 binding to NRG1ab, respectively. In plasma, these values were estimated to 201 and 30 pM, respectively.

To compare the results obtained with liposome-enhanced SPR (Figure 2), we also used the ultrasensitive Erenna microbead-based single-molecule detection platform for NRG1. Figure 4C shows the dose−response curves for NRG1 when interacted with ErbB4 and NRG1ab that were labeled with AL647, both in buffer and plasma conditions. In Figure 4D, the corresponding linear regression fits for NRG1 quantification are shown. With the Erenna immunoassay, we obtained LOD of 28 pM for NRG1 when ErbB4 was the detection analyte in buffer. This value did not shift much in plasma samples (LOD = 40 pM). As expected, antibody NRG1 showed more potency and we could detect 2 pM of Fc-NRG1 as a LOD in buffer and down to 7.4 pM of Fc-NRG1 in plasma samples.

Detection of molecular biomarkers typically requires access to pairs of specific, high-affinity antibodies that involve mutually inclusive binding to generate a measurable signal. Finding a matching and fruitful combination of high affinity antibodies is the key for achieving the required specificity and sensitivity. Albeit most antibodies are typically not conformation-sensitive and thus do not inform about the functional state of the biomarker, this information can be expected to be of

DOI: 10.1021/acssensors.9b01392
ACS Sens. 2019, 4, 3166−3174

Table 2. Detection Limit for NRG1 Using Different Methods[a]

method	ErbB4 buffer (pM)		ErbB4 plasma (pM)		NRG1ab buffer (pM)		NRG1ab plasma (pM)	
	LOD	LOQ	LOD	LOQ	LOD	LOQ	LOD	LOQ
SPR	200	666	nd	nd	na	na	na	na
Gyrolab	198	660	201	671	0.6	2.0	30	102
Singulex	28	94.6	40	134	2.0	6.6	7.4	25
liposome-amplified SPR	3.5	12	36	120	na	na	na	na

[a]nd = not determined; na = not applicable; LOD = limit of detection; LOQ = limit of quantification.

high physiological relevance. Whilst this in theory can be achieved via functional reporters, their lower affinity and transient binding properties makes them unsuitable for highly sensitive detection purposes. The employed assay architecture makes use of liposomes coated with multiple functional binders, thereby eliminating this shortcoming through a combination of liposome-mediated avidity and signal amplification.

Fusing the Fc domain of an IgG to a receptor protein, peptide, cytokine, or antibody domain is a typical strategy to increase the plasma-half-life of such a Fc-fusion protein if considered as a biologic.[34,35] Many of these Fc-fusion proteins and monoclonal antibodies have been approved for marketing and more are currently in clinical trials as a result of their extended half-life in circulation that permits less frequent dose administration and more effective therapeutics.[36,37] In addition, the Fc region can also serve to provide a defined orientation on a biosensor surface.[38] In this study, the Fc-region on the NRG1 serves as an epitope for the first antibody that captures the analyte and brings it in an orientation to interrogate the active concentration of the biomarker.

In this work, we show the avidity effect for the interaction between NRG1 and its functional interaction ErbB4 being coated on liposomes fulfilling the combined purpose of a signal amplifier and increased affinity. This was shown to enable 4 orders of magnitude higher affinity, attributed to consecutive rebinding events of liposome-attached ErbB4 molecules to multiple NRG1. In fact, the dissociation rate with the liposome employed assay (Figure 2C) is comparable to the dissociation rate of the high affinity antibody (Figure 2B). We attribute the apparent biphasic pattern during dissociation of ErbB4-decorated liposomes to heterogeneity in the ErbB4 coverage on different liposomes.[39] This deviation from the theoretical mono-exponential release rate hinders a correct quantification of residence time of the ligand. However, because the liposome-amplified NRG1 and ErbB4 interactions do not reach equilibrium, it is reasonable to assume that the K_d values for the interaction between NRG1 and ErbB4-coated liposomes are orders of magnitude lower than for the monovalent NRG1 and ErbB4 interactions. Indeed, the observed affinity between NRG1 and ErbB4 is boosted at least 4 orders of magnitude, approaching low picomolar affinity when ErbB4 molecules are coated on the liposomes (Table 1), thus approaching the high-affinity interaction observed between NRG1 and NRG1ab. This observed affinity enhancement appears to be a direct consequence of a decrease in the rate of dissociation. Such frequent observations for high-affinity polyvalent interactions can be mainly attributed to the high thermodynamic cost for simultaneously breaking multiple interactions between the two polyvalent species.[40,41] However, the thermodynamic cost for building up the first interaction during the association process is almost the same for polyvalent ligand−receptor interactions as compared to the analogous monovalent interactions, suggesting that association rates will be fairly similar. This is in fact supported by our data as shown in Table 1. In summary, the dissociation of polyvalently interacting species requires breaking of a larger number of ligand−receptor interactions, which causes slower dissociation in the case of polyvalent interactions as compared to monovalent interactions.[40] This is the main origin for the observed affinity enhancement.

In Table 2, we summarized the LOD and limit of quantification (LOQ, calculated from 10σ/slope) for four different detection platforms. LOQ is originally developed as a clinical diagnostic tool and thus more applicable in pharma industry compared to LOD.[42] LOD and LOQ for NRG1 when interacting with its natural receptor ErbB4 using liposome-amplified SPR corresponds to 3.5 and 12 pM, respectively. This sensitivity is about 60 times higher than the traditional SPR (LOQ = 666 pM) and miniaturized immunoassay with Gyrolab (LOQ = 660 pM). When comparing the sensitivity with highly sensitive single-molecule Erenna immunoassay (LOQ = 94.6 pM), our biosensor showed 8 times higher sensitivity. Liposome-enhanced SPR allowed us to measure NRG1 in plasma samples (LOQ = 120 pM) with a sensitivity that is in the same order of magnitude as the single-molecule Erenna immunoassay (LOQ = 134 pM) and hence much lower than the Gyrolab immunoassay (LOQ = 671 pM). Although not necessarily representing the functional state of the detected biomarkers, antibodies are from the perspective of reaching low LODs more potent than natural receptors. We therefore measured the interaction between NRG1 and NRG1ab using the Gyrolab and Singulex platforms (Table 2). With these techniques, the detection sensitivity for Fc-NRG1 when employing a high affinity antibody was comparable to our liposome-enhanced SPR, although the natural receptor ErbB4 exhibits 4 orders of magnitude lower affinity.

In the context of comparisons of LODs and LOQs using different binders and platforms, it is relevant to recall, that the dissociation rate for NRG1 and ErbB4 (Figure 2A) was 3 orders of magnitudes lower for ErbB4-coated liposomes (Figure 2C) and approaches the antibody dissociation rate (Figure 2B). This is a much more comparable parameter as it reflects the evidence of functional avidity. Moreover, the observed affinity between NRG1 and ErbB4 is boosted at least 3 orders of magnitude for the liposome assay and come close to the low picomolar regime (Table 1). Further, although in this work serving as a functional reporter for NRG1 detection, ErbB4 is in its own right a critical biomarker, and thus its detection can be vital for early diagnosis of several cancer types.[13,14] To this end, we reversed the detection platform proposed in Figure 1A and measured ErbB4 concentrations from the dose−response curves as shown in Figure S7. LOD for ErbB4 when bound to liposomes is calculated as 32.8 pM from the linear regression curve.

DOI: 10.1021/acssensors.9b01392
ACS Sens. 2019, 4, 3166−3174

CONCLUSIONS

The developed liposome-enhanced biomarker detection approach based on SPR displays sensitivities in the range of single-molecule digital platforms without requiring a fluorescent label or a high-affinity secondary antibody. It enables the detection of low-affinity natural binding partners via functional affinity, which through liposome-induced avidity effects lead to comparable binding affinities to those offered by high-affinity antibodies. To the best of our knowledge, this is the first biosensor for the detection of NRG1 and ErbB4 at low-picomolar LOD without a fluorescent readout. It is worth noting, that the phospholipid vesicles that have been employed as signal enhancers also mimick the cell membrane surface. The proposed sensor is thus suitable and compatible with a wide variety of biomarker−receptor pairs that can be either soluble or membrane-bound. Equally important, the generic setup and approach of this strategy allows an effective transfer to a whole range of other biomarker systems. As liposomes very much resemble the architecture of exosomes, it appears to be highly feasible to use exosomes for the detection of surface-exposed biomarkers with the aim of addressing different biological matrices. In another step, one can also explore the dynamics of low-affinity binding antibodies and receptors using single-molecule fluorescence microscopy, furnishing the opportunity to further increase the current sensitivity obtained by liposome-enhanced SPR by several orders of magnitude. The deployment of a more sensitive single-molecule platform will further increase the technical feasibility around the expected sensitivity gains. By simultaneously focusing on a wider set of challenging biomarkers, this biosensor platform will further ensure the generation of significant scientific impact in an area of high diagnostic need. Finally, we used in this work a commercial SPR system with integrated microfluidics and fully automated liquid handling designed for high-throughput drug discovery. However, the added value of the liposome-enhancement assay is not dependent on these features, thus ensuring full compatibility with most types of optical biosensor detection principles. Given the rapid development of simplified SPR systems focusing on point of care application,[43] our contribution may thus become valuable far beyond functional analysis of rare and sensitive biologics as it ensures detection of biomarkers in their functional state while simultaneously opening for the use of a more versatile set of inherently weak binders.

ASSOCIATED CONTENT

Supporting Information

The Supporting Information is available free of charge at https://pubs.acs.org/doi/10.1021/acssensors.9b01392.

Liposome size, optimization of the sensor conditions, SPR data in plasma samples, and ErbB4 biosensor (PDF)

AUTHOR INFORMATION

Corresponding Author

*E-mail: Stefan.Geschwindner@astrazeneca.com.

ORCID

Fredrik Höök: 0000-0003-1994-5015

Stefan Geschwindner: 0000-0002-2154-8345

Author Contributions

The manuscript was written through contributions of all authors. All authors have given approval to the final version of the manuscript.

Notes

The authors declare the following competing financial interest(s): AstraZeneca authors are current or former salaried employees of AstraZeneca and have/had stock or stock options in AstraZeneca.

ACKNOWLEDGMENTS

N.A. is supported by the AstraZeneca postdoc programme. FH is supported by the Swedish Research Council (grant no 2018-04900). We thank Gerard Donohoe for antibody validation, Eileen McCall for expression of NRG1 antibody constructs, Kelly Hearne and Liam Hutchinson for purification of the NRG1 antibodies.

REFERENCES

(1) Atkinson, A.; Colburn, W.; Degruttola, V.; Demets, D.; Downing, G.; Hoth, D.; Oates, J.; Peck, C.; Schooley, R.; Spilker, B.; Woodcock, J.; Zeger, S. Biomarkers and surrogate endpoints: Preferred definitions and conceptual framework. *Clin. Pharmacol. Ther.* **2001**, *69*, 89−95.

(2) Yap, T. A.; Sandhu, S. K.; Workman, P.; de Bono, J. S. Envisioning the future of early anticancer drug development. *Nat. Rev. Cancer* **2010**, *10*, 514.

(3) Zhang, P.; Kuang, H.; He, Y.; Idiga, S. O.; Li, S.; Chen, Z.; Yang, Z.; Cai, X.; Zhang, K.; Potthoff, M. J.; Xu, Y.; Lin, J. D. NRG1-Fc improves metabolic health via dual hepatic and central action. *JCI Insight* **2018**, *3*, No. e98522.

(4) Nave, K.-A.; Trapp, B. D. Axon-Glial Signaling and the Glial Support of Axon Function. *Annu. Rev. Neurosci.* **2008**, *31*, 535−561.

(5) Mei, L.; Nave, K.-A. Neuregulin-ERBB Signaling in the Nervous System and Neuropsychiatric Diseases. *Neuron* **2014**, *83*, 27−49.

(6) Gassmann, M.; Casagranda, F.; Orioli, D.; Simon, H.; Lai, C.; Klein, R.; Lemke, G. Aberrant neural and cardiac development in mice lacking the ErbB4 neuregulin receptor. *Nature* **1995**, *378*, 390.

(7) Wadugu, B.; Kühn, B. The role of neuregulin/ErbB2/ErbB4 signaling in the heart with special focus on effects on cardiomyocyte proliferation. *Am. J. Physiol.: Heart Circ. Physiol.* **2012**, *302*, H2139−H2147.

(8) Hahn, C.-G.; Wang, H.-Y.; Cho, D.-S.; Talbot, K.; Gur, R. E.; Berrettini, W. H.; Bakshi, K.; Kamins, J.; Borgmann-Winter, K. E.; Siegel, S. J.; Gallop, R. J.; Arnold, S. E. Altered neuregulin 1-erbB4 signaling contributes to NMDA> receptor hypofunction in schizophrenia. *Nature Medicine* **2006**, *12*, 824.

(9) Mei, L.; Xiong, W.-C. Neuregulin 1 in neural development, synaptic plasticity and schizophrenia. *Nat. Rev. Neurosci.* **2008**, *9*, 437.

(10) Takahashi, Y.; Fukuda, Y.; Yoshimura, J.; Toyoda, A.; Kurppa, K.; Moritoyo, H.; Belzil, V. V.; Dion, P. A.; Higasa, K.; Doi, K.; Ishiura, H.; Mitsui, J.; Date, H.; Ahsan, B.; Matsukawa, T.; Ichikawa, Y.; Moritoyo, T.; Ikoma, M.; Hashimoto, T.; Kimura, F.; Murayama, S.; Onodera, O.; Nishizawa, M.; Yoshida, M.; Atsuta, N.; Sobue, G.; Fifita, J. A.; Williams, K. L.; Blair, I. P.; Nicholson, G. A.; Gonzalez-Perez, P.; Brown, R. H.; Nomoto, M.; Elenius, K.; Rouleau, G. A.; Fujiyama, A.; Morishita, S.; Goto, J.; Tsuji, S. ERBB4 Mutations that Disrupt the Neuregulin-ErbB4 Pathway Cause Amyotrophic Lateral Sclerosis Type 19. *Am. J. Hum. Genet.* **2013**, *93*, 900−905.

(11) Jiang, Q.; Chen, S.; Hu, C.; Huang, P.; Shen, H.; Zhao, W. Neuregulin-1 (Nrg1) signaling has a preventive role and is altered in the frontal cortex under the pathological conditions of Alzheimer's disease. *Mol. Med. Rep.* **2016**, *14*, 2614−2624.

(12) Michailov, G. V.; Sereda, M. W.; Brinkmann, B. G.; Fischer, T. M.; Haug, B.; Birchmeier, C.; Role, L.; Lai, C.; Schwab, M. H.; Nave, K.-A. Axonal Neuregulin-1 Regulates Myelin Sheath Thickness. *Science* **2004**, *304*, 700−703.

DOI: 10.1021/acssensors.9b01392
ACS Sens. 2019, 4, 3166−3174

(13) Tang, C. K.; Concepcion, X.-Z. W.; Milan, M.; Gong, X.; Montgomery, E.; Lippman, M. E. Ribozyme-mediated Down-Regulation of ErbB-4 in Estrogen Receptor-positive Breast Cancer Cells Inhibits Proliferation Both in Vitro and in Vivo. *Cancer Res.* **1999**, *59*, 5315−5322.
(14) Veikkolainen, V.; Vaparanta, K.; Halkilahti, K.; Iljin, K.; Sundvall, M.; Elenius, K. Function ofERBB4is determined by alternative splicing. *Cell Cycle* **2011**, *10*, 2647−2657.
(15) Cowan, K. J.; Geiger, A.; Hornauer, H.; Rourick, R.; Siguenza, P. Y. Performance evaluation of three platforms with ultrasensitive ligand-binding assay potential. *Bioanalysis* **2017**, *9*, 937−946.
(16) Fischer, S. K.; Joyce, A.; Spengler, M.; Yang, T.-Y.; Zhuang, Y.; Fjording, M. S.; Mikulskis, A. Emerging technologies to increase ligand binding assay sensitivity. *AAPS J.* **2014**, *17*, 93−101.
(17) Todd, J.; Freese, B.; Lu, A.; Held, D.; Morey, J.; Livingston, R.; Goix, P. Ultrasensitive Flow-based Immunoassays Using Single-Molecule Counting. *Clin. Chem.* **2007**, *53*, 1990−1995.
(18) Shukla, R.; Santoro, J.; Bender, F. C.; Laterza, O. F. Quantitative determination of human interleukin 22 (IL-22) in serum using Singulex-Erenna Technology. *J. Immunol. Methods* **2013**, *390*, 30−34.
(19) Gauvreau, G. M.; Boulet, L.-P.; Cockcroft, D. W.; FitzGerald, J. M.; Carlsten, C.; Davis, B. E.; Deschesnes, F.; Duong, M.; Durn, B. L.; Howie, K. J.; Hui, L.; Kasaian, M. T.; Killian, K. J.; Strinich, T. X.; Watson, R. M.; Y, N.; Zhou, S.; Raible, D.; O'Byrne, P. M. Effects of Interleukin-13 Blockade on Allergen-induced Airway Responses in Mild Atopic Asthma. *Am. J. Respir. Crit. Care Med.* **2011**, *183*, 1007−1014.
(20) Rissin, D. M.; Kan, C. W.; Campbell, T. G.; Howes, S. C.; Fournier, D. R.; Song, L.; Piech, T.; Patel, P. P.; Chang, L.; Rivnak, A. J.; Ferrell, E. P.; Randall, J. D.; Provuncher, G. K.; Walt, D. R.; Duffy, D. C. Single-Molecule enzyme-linked immunosorbent assay detects serum proteins at subfemtomolar concentrations. *Nat. Biotechnol.* **2010**, *28*, 595−599.
(21) Wilson, D. H.; Rissin, D. M.; Kan, C. W.; Fournier, D. R.; Piech, T.; Campbell, T. G.; Meyer, R. E.; Fishburn, M. W.; Cabrera, C.; Patel, P. P.; Frew, E.; Chen, Y.; Chang, L.; Ferrell, E. P.; von Einem, V.; McGuigan, W.; Reinhardt, M.; Sayer, H.; Vielsack, C.; Duffy, D. C. The Simoa HD-1 Analyzer. *J. Lab. Autom.* **2016**, *21*, 533−547.
(22) Song, L.; Lachno, D. R.; Hanlon, D.; Shepro, A.; Jeromin, A.; Gemani, D.; Talbot, J. A.; Racke, M. M.; Dage, J. L.; Dean, R. A. A digital enzyme-linked immunosorbent assay for ultrasensitive measurement of amyloid-β 1−42 peptide in human plasma with utility for studies of Alzheimer's disease therapeutics. *Alzheimer's Res. Ther.* **2016**, *8*, 58.
(23) Leirs, K.; Tewari Kumar, P.; Decrop, D.; Pérez-Ruiz, E.; Leblebici, P.; Van Kelst, B.; Compernolle, G.; Meeuws, H.; Van Wesenbeeck, L.; Lagatie, O.; Stuyver, L.; Gils, A.; Lammertyn, J.; Spasic, D. Bioassay Development for Ultrasensitive Detection of Influenza A Nucleoprotein Using Digital ELISA. *Anal. Chem.* **2016**, *88*, 8450−8458.
(24) Gaylord, S. T.; Abdul-Aziz, S.; Walt, D. R. Single-Molecule Arrays for Ultrasensitive Detection of Host Immune Response to Dengue Virus Infection. *J. Clin. Microbiol.* **2015**, *53*, 1722−1724.
(25) Rissin, D. M.; Kan, C. W.; Song, L.; Rivnak, A. J.; Fishburn, M. W.; Shao, Q.; Piech, T.; Ferrell, E. P.; Meyer, R. E.; Campbell, T. G.; Fournier, D. R.; Duffy, D. C. Multiplexed single molecule immunoassays. *Lab Chip* **2013**, *13*, 2902−2911.
(26) Li, W.; Jiang, W.; Dai, S.; Wang, L. Multiplexed Detection of Cytokines Based on Dual Bar-Code Strategy and Single-Molecule Counting. *Anal. Chem.* **2016**, *88*, 1578−1584.
(27) Cohen, L.; Walt, D. R. Single-Molecule Arrays for Protein and Nucleic Acid Analysis. *Annu. Rev. Anal. Chem.* **2017**, *10*, 345−363.
(28) Fenzl, C.; Hirsch, T.; Baeumner, A. J. Liposomes with High Refractive Index Encapsulants as Tunable Signal Amplification Tools in Surface Plasmon Resonance Spectroscopy. *Anal. Chem.* **2015**, *87*, 11157−11163.
(29) Gunnarsson, A.; Snijder, A.; Hicks, J.; Gunnarsson, J.; Höök, F.; Geschwindner, S. Drug Discovery at the Single Molecule Level: Inhibition-in-Solution Assay of Membrane-Reconstituted β-Secretase Using Single-Molecule Imaging. *Anal. Chem.* **2015**, *87*, 4100−4103.
(30) Bouyain, S.; Longo, P. A.; Li, S.; Ferguson, K. M.; Leahy, D. J. The extracellular region of ErbB4 adopts a tethered conformation in the absence of ligand. *Proc. Natl. Acad. Sci. U.S.A.* **2005**, *102*, 15024−15029.
(31) Ferguson, K. M.; Darling, P. J.; Mohan, M. J.; Macatee, T. L.; Lemmon, M. A. Extracellular domains drive homo- but not hetero-dimerization of erbB receptors. *EMBO J.* **2000**, *19*, 4632−4643.
(32) Vauquelin, G.; Charlton, S. J. Exploring avidity: understanding the potential gains in functional affinity and target residence time of bivalent and heterobivalent ligands. *Br. J. Pharmacol.* **2013**, *168*, 1771−1785.
(33) Hill, A. V. The possible effects of the aggregation of the molecules of hæmoglobin on its dissociation curves. *J. Physiol.* **1910**, *40*, i−vii.
(34) Strohl, W. R. Fusion Proteins for Half-Life Extension of Biologics as a Strategy to Make Biobetters. *BioDrugs* **2015**, *29*, 215−239.
(35) Lagassé, H. A. D.; Alexaki, A.; Simhadri, V. L.; Katagiri, N. H.; Jankowski, W.; Sauna, Z. E.; Kimchi-Sarfaty, C. Recent advances in (therapeutic protein) drug development. *F1000Research* **2017**, *6*, 113.
(36) Czajkowsky, D. M.; Hu, J.; Shao, Z.; Pleass, R. J. Fc-fusion proteins: new developments and future perspectives. *EMBO Mol. Med.* **2012**, *4*, 1015−1028.
(37) Baker, K.; Dumont, J. A.; Peters, R. T.; Jiang, H.; Qiao, S.-W.; Lencer, W. I.; Pierce, G. F.; Blumberg, R. S. Fc-fusion proteins and FcRn: structural insights for longer-lasting and more effective therapeutics. *Crit. Rev. Biotechnol.* **2015**, *35*, 235−254.
(38) Yan, H.; Shen, Z.; Mernaugh, R.; Zeng, X. Single Chain Fragment Variable Recombinant Antibody as a Template for Fc Sensors. *Anal. Chem.* **2011**, *83*, 625−630.
(39) Bally, M.; Gunnarsson, A.; Svensson, L.; Larson, G.; Zhdanov, V. P.; Höök, F. Interaction of Single Viruslike Particles with Vesicles Containing Glycosphingolipids. *Phys. Rev. Lett.* **2011**, *107*, 188103.
(40) Mammen, M.; Choi, S.-K.; Whitesides, G. M. Polyvalent Interactions in Biological Systems: Implications for Design and Use of Multivalent Ligands and Inhibitors. *Angew. Chem., Int. Ed.* **1998**, *37*, 2754−2794.
(41) Karush, F. The Affinity of Antibody: Range, Variability, and the Role of Multivalence. *Immunoglobulins*; Springer, 1978; Vol. *5*, pp 85−116.
(42) Armbruster, D. A.; Pry, T. Limit of blank, limit of detection and limit of quantitation. *Clin. Biochem. Rev.* **2008**, *29*, S49−S52.
(43) Peltomaa, R.; Glahn-Martínez, B.; Benito-Peña, E.; Moreno-Bondi, M. Optical Biosensors for Label-Free Detection of Small Molecules. *Sensors* **2018**, *18*, 4126.

DOI: 10.1021/acssensors.9b01392
ACS Sens. 2019, 4, 3166−3174